Batteries & Supercaps

Research Article
doi.org/10.1002/batt.202200499

Chemistry Europe
European Chemical Societies Publishing

www.batteries-supercaps.org

Oriented-Etched Graphite for Low-Temperature Lithium-Ion Batteries

Jiang Xu,[a] Xuanding Wang,[a] Bingqing Hu,[a] Jianning Ding,[a, b] Zhongqiang Zhang,*[a] and Shanhai Ge*[c]

As an environmentally friendly energy storage media, lithium-ion batteries have been extensively used and investigated. However, fast-charging and low-temperature tolerance are still huge challenges for the graphite-based batteries. To alleviate the poor rate performance caused by long diffusion path and the risk of lithium dendrite growth at high rate or low temperature charging, graphite with penetrated macropores is fabricated here, combined with ether-based electrolyte with low solvation energy, the smooth migration of Li^+/Li at the electrolyte-electrode interface and interior of the graphite is ensured. The product graphite exhibits excellent rate and low-temperature performance, evidenced by 352.9 mAh g^{-1} capacity delivered at 2 C-rate and −30 °C. In addition, benefited from the intact preservation of the pristine graphite structure, it exhibits ~85% initial charge-discharge efficiency and long cycle life (~94.2% capacity retention after 500 cycles). This synergic strategy makes the product graphite very efficient in the fast charging/discharging and low temperature occasions.

Introduction

Lithium-ion batteries (LIBs) are widely used in portable devices, electric vehicles, and renewable power stations.[1–3] As an important part of LIBs, graphite anode played a dominated role in the past 30 years owing to its high Li^+ storage capacity (372 mAh g^{-1}), low cost, high energy density and good reversibility.[4,5] However, the graphite anode is considered to be the main culprit that limits the high-rate charging of commercial LIBs.[6] On one hand, graphite owns a low lithiation potential (~0.1 V vs. Li/Li^+). Thus, various polarizations at graphite anode would lead the potential of the electrode under the threshold of metal Li plating, especially under high rate and low temperature lithiation process, which would greatly affect the safety of the cell. On the other hand, high anisotropy of graphite leads to a distinct Li^+ diffusion constant in different directions (e.g., ~10^{-7}–10^{-6} $cm^2 s^{-1}$ in in-plane direction and ~10^{-11} $cm^2 s^{-1}$ in through-plane direction).[7] Thus, Li^+ can only intercalate into graphite through the in-plane direction and diffuse slowly among the graphite layers (Figure 1a), which would severely restrict the applications of commercial LIBs at high rate or low temperature occasions.[8–10]

Previous experimental efforts to improve rate performance of graphite include modification of graphite structure or its surface.[11–15] Li^+/Li diffusion is promoted in the graphite and at the interface through reducing the Li^+ diffusion distance and increasing the intercalation surface. However, due to the graphite with both high orientation and stability, it would be very hard to form evenly distributed channels in the normal direction of graphite by simple physical or chemical activation. In addition, these surface modifications might increase its surface area. However, higher specific surface area of electrode would lead lower initial Coulombic efficiency (ICE) and higher rate of heat generation.[12,16–19] To reduce the irreversible capacity loss at first cycle and the thermal runaway hazard at following cycles of LIB, the specific surface area of graphite should not be high.

Herein, we fabricate macroporous graphite (denoted as MPG) containing numerous penetrated pores with size of ~100 nm, using physical activation assisted by metal oxide (Figure 1c). As depicted in Figure 1(b), ions could intercalate into the porous graphite particle from different directions. Furthermore, to alleviate the hysteresis of ion de-solvation at the interface[20–22] at high C-rate or low temperature, an electrolyte with low de-solvation energy [1,3-dioxolane (DOL), ethylene carbonate (EC) and vinylene carbonate (VC) (96:2:2 vol%), denoted as DEV] is applied in this work. Benefited from the new electrode-electrolyte combination, the product graphite anode exhibits both high rate and low-temperature tolerant performance. In addition, it also shows high ICE and excellent cycling stability. The presented strategy can be used to design robust graphite-based LIBs with high power at all temperatures.

[a] Dr. J. Xu, X. Wang, B. Hu, Prof. J. Ding, Prof. Z. Zhang
Institute of Intelligent Flexible Mechatronics
Jiangsu University
Zhenjiang 212013 (P. R. China)
E-mail: zhangzq@ujs.edu.cn
[b] Prof. J. Ding
School of Mechanical Engineering
Yangzhou University
Yangzhou 225127 (P. R. China)
[c] Prof. S. Ge
Department of Mechanical Engineering
The Pennsylvania State University, University Park
Pennsylvania 16802 (USA)
E-mail: sug13@psu.edu

Supporting information for this article is available on the WWW under https://doi.org/10.1002/batt.202200499

Research Article
doi.org/10.1002/batt.202200499
Chemistry Europe
European Chemical Societies Publishing

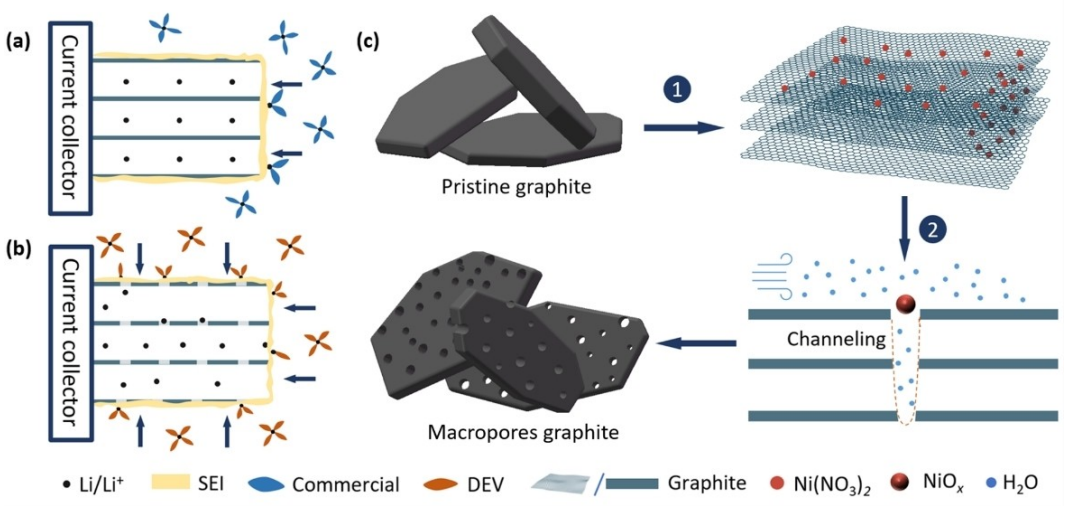

Figure 1. Schematic illustration of Li^+ intercalation process for a) the pristine graphite in the commercial electrolyte, and b) MPG in DOL based electrolyte (DEV), c) the preparation process of macroporous graphite (MPG). Step 1: stirring with $Ni(NO_3)_2$ and spry drying. Step 2: steam activation.

Results and Discussion

Structure characterization

To ensure the uniformity of the activation, spray-drying was introduced to load the activator on the surface of the pristine graphite particles. As shown in Figure S1, $Ni(NO_3)_2$ was evenly distributed on the surface of the graphite particles. The structural difference of the graphite before and after activation is shown in Figure 2(a–d). Apparently, the surface of the pristine graphite is compact and smooth (Figure 2a). After activating, many macropores with size of about 100 nm were formed in MPG (Figure 2b). The magnified scanning electron microscopy (SEM) image and transmission electron microscopy (TEM) image further indicate that these macropores are thoroughly penetrated (Figure 2c and d). The left side of the red dash line in Figure 2(d) is TEM image of MPG, which shows that the size of the pores is about 100 nm in average and evenly distributed in MPG. And the smooth circles at the top right are the TEM image of the lacey support film. This benefited from the catalytic behavior of the transition metal oxide, originating from the following equations:

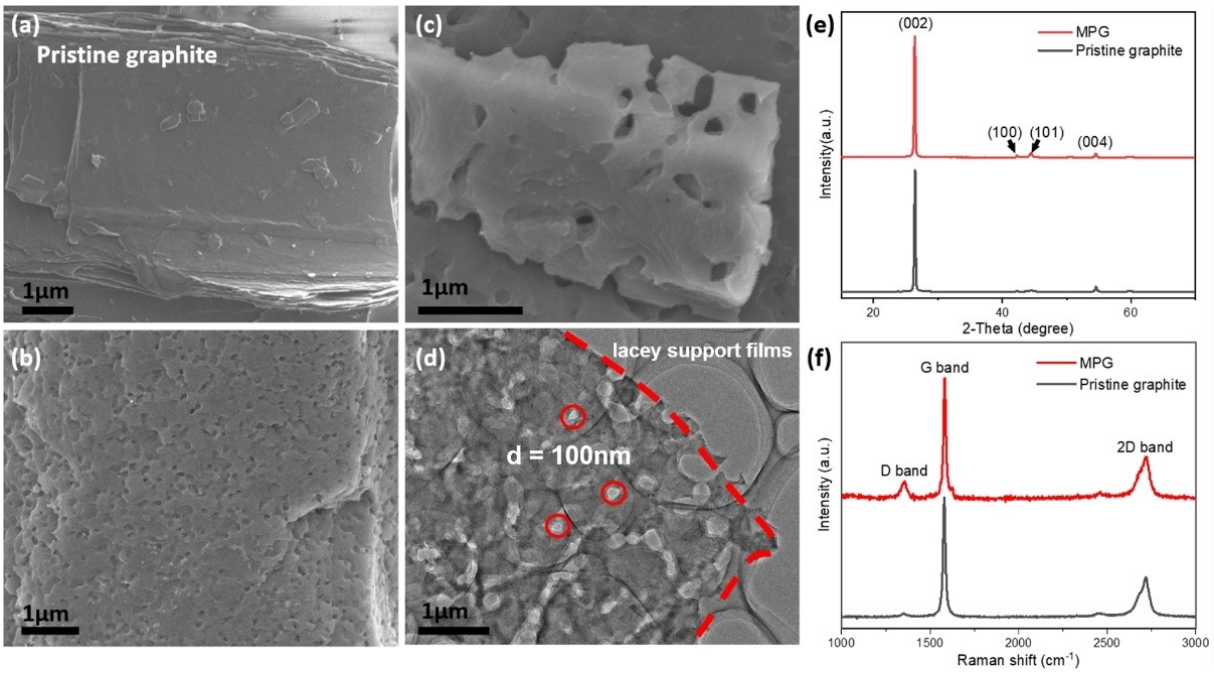

Figure 2. SEM images of a) the pristine graphite and b, c) MPG. d) TEM image of MPG. e) XRD patterns and f) Raman spectra of the pristine graphite and MPG.

Research Article
doi.org/10.1002/batt.202200499
Chemistry Europe
European Chemical Societies Publishing

$$Ni(NO_3)_2 \rightarrow NiO_x + NO_2 + O_2 \quad (1)$$

$$C + H_2O \rightarrow CO + H_2 \quad (2)$$

According to Equation (1), $Ni(NO_3)_2$-graphite would gradually transform to NiO_x-graphite when the temperature is over 500 °C.[23] With the temperature further increasing to 900 °C, the pumped steam would react with graphite in the presence of the NiO_x catalyst and form penetrated pores in graphite following Equation (2). Since a high activation energy is needed for the reaction between C and H_2O, the area without NiO_x catalyst would be well maintained under a mild temperature (< 1000 °C). In addition, only a small amount of Ni/NiO_x (less than 0.1 %) remains on the surface and the lateral of the final MPG production (Figure S2).

In order to further investigate the effect of activation on the microstructure of graphite, X-ray diffusion (XRD) and Raman spectroscopy are adopted to analyse the crystal structure of the synthesized sample.[24,25] As shown in Figure 2(e), similar (002) peaks in MPG and the pristine graphite indicate that the crystal structure of the pristine graphite is not damaged after activating. Whereas for Raman spectra, a notable difference between MPG and the pristine graphite can be detected (Figure 2f). Due to its remarkable sensitivity to the defects of graphite, Raman spectroscopy is widely used to evaluate the structural change of carbon materials.[26] As shown in Figure 2(f), the intensity of the disordered-induced D band increases after activating. This indicates that more defects and disordered structures exist in MPG. In addition, there is little difference between the spectra of the pristine graphite and the activated graphite without activator (Figure S3). The increased defects in MPG can be attributed to the edge of the etched pores. Thus, it can be concluded that the pristine graphite can be etched directionally by steam at a moderate temperature with the existence of NiO_x and consequently form graphite with penetrated macropores. As shown in Figure S4, the specific surface area of the graphite increases from 1.8 $m^2 g^{-1}$ to 23 $m^2 g^{-1}$ after activation. The extra surface area could decrease battery thermal stability and increase the irreversible capacity loss in SEI formation process. However, due to the highly pressed of the electrode (1.4 $g cm^{-3}$), the electrochemical surface area would not be high.

Electrochemical characterization

The merit of MPG for LIBs was further demonstrated by its electrochemical performance, as shown in Figure 3. MPG displays a typical cyclic voltammetry (CV) curve of graphite.[21,27] During the first discharge (lithiation) process, there is a clear broad reductive peak located in the range of 0.85 to 0.65 V,

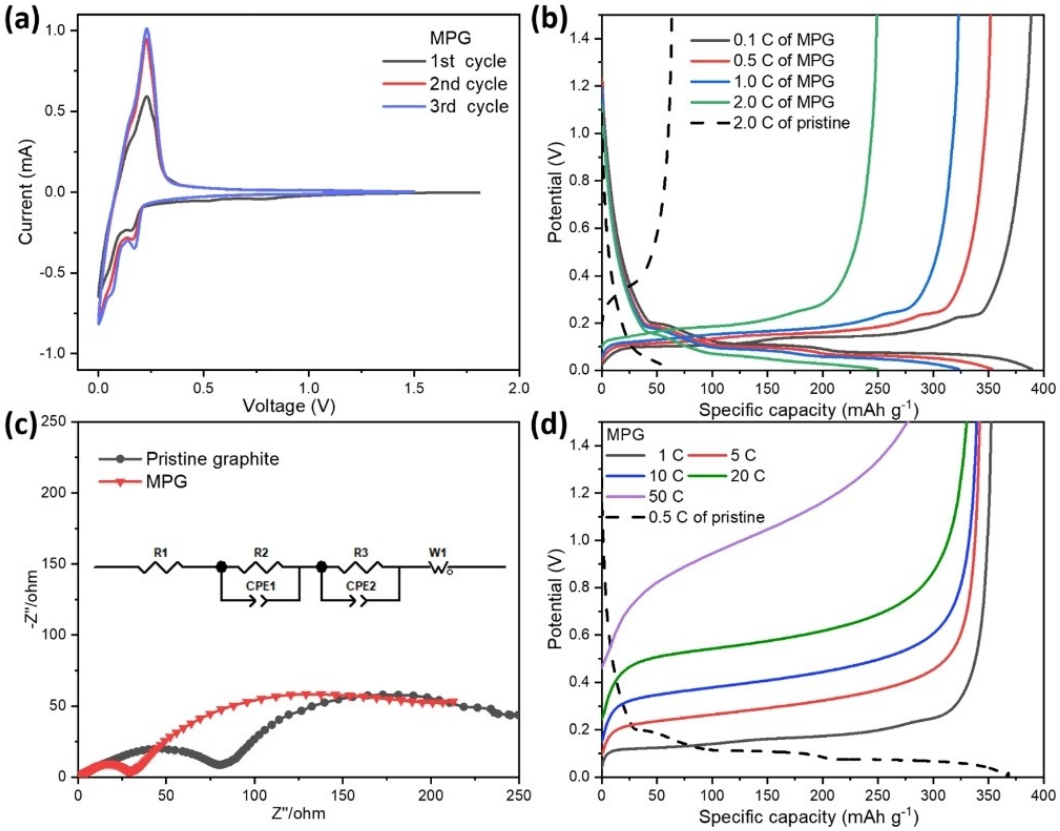

Figure 3. Electrochemical tests of MPG measured at room temperature in the commercial electrolyte: a) CV curves of the initial 3 cycles measured at a scan rate of 0.05 mV s^{-1}. b) galvanostatic charge/discharge (GCD) curves of MPG measured at different rates. c) Electrochemical impedance spectroscopies of MPG and the pristine graphite. d) Li-output curves of MPG measured at different C rates after 0.5 C lithium insertion.

Research Article
doi.org/10.1002/batt.202200499
Chemistry Europe
European Chemical Societies Publishing

which is believed to be the electrolyte decomposition and concomitant solid-electrolyte interface (SEI) formation.[21,27–29] In the subsequent lithiation process, the appearance of the peaks located at 0.16 and 0.05 V are ascribed to the formation of LiC_x ($x>6$) intermediates.[21] For the anodic scan, three peaks at about 0.15, 0.23 and 0.27 V correspond to the stepwise de-lithiation process from LiC_x intermediates to C.[21,27] These peaks correspond well with those obtained in the commercial graphite,[28,30] benefiting from the well-maintained graphitic lattice structure in MPG displayed above (Figure 2).

The electrochemical lithium storage properties of MPG were evaluated by galvanostatic discharge-charge measurement. Figure 3(b) shows discharge-charge profiles of MPG measured at room temperature with different C-rates of 0.1, 0.5, 1 and 2. Notably, the specific capacity of MPG measured at 0.1 C-rate exceeds the theoretical capacity of the typical graphite, which can be accounted for the Li adsorption of the additional defects and disorder structures in MPG.[31] Although the capacity of MPG decreases gradually with increasing rates, three pairs of the typical lithiation/de-lithiation plateaus of the graphite can be clearly detected in MPG even at 2 C-rate, which is in agreement well with the redox peaks exhibited in the CV curves. Whereas for the pristine graphite, the capacity retention decreases sharply and only about 50 mAh g^{-1} capacity can be delivered at 2 C-rate (Figures 3b, S5 and S6). In order to explore the influence of macropores on the ion migration, electrochemical impedance spectroscopy (EIS) tests were employed. Before EIS tests, all cells were galvanostatic discharged and charged at 0.2 C-rate for 10 cycles and then discharged to 0.079 V at room temperature. As shown in Figure 3(c), there is a notable difference between the pristine graphite and MPG, especially for the semicircle located in the medium frequency region.[10,32] The smaller value of charge-transfer resistance (R_{ct}) for MPG illustrates that MPG owns a lower interfacial impedance resistance than the pristine graphite during Li^+ intercalation process, which might be attributed to the increased active surface from the penetrated macropores. Due to intercalation potential vs. Li is close to 0 V, the graphite/Li half-cell is not suitable to evaluate the lithiation rate capability.[12,33] Thus, we measured Li-output performance of MPG electrode at various rates from 1 to 50 C (Figure 3d). It shows that the Li-output capacity of MPG in half cell could reach about 280 mAh g^{-1} at 50 C. Though the rate performance of the pristine graphite lags behind MPG, it can still deliver ~250 mAh g^{-1} capacity at 10 C (Figures S7 and S8). This can be deduced that the charge-transfer resistance at interface is mainly caused by the hysteretic de-solvation rate of the solvated Li^+.

To alleviate the impediment of Li^+ intercalation process, DOL with weak polar is used as solvent in this work to promote the de-solvation process of the solvated ions at liquid-solid interface.[10,33,34] Moreover, 2% EC[7] and 2% VC (by volume) are employed as additives to form a compact SEI layer on the surface of MPG, thereby ensuring cycle stability.[35] As shown in Figure 4(a), the initial three cycling curves of MPG measured in DEV have more clear reductive peaks (0.83, 0.17, 0.05 V) than that measured in the commercial electrolyte. In addition, it is noted that a higher overlap rate is detected between the first and the second cycling curves of MPG measured in DEV. This might be benefited from the improved wettability of MPG electrode in DEV electrolyte. As shown in Figure 4(b), MPG electrode is well immersed in DEV electrolyte and a smaller

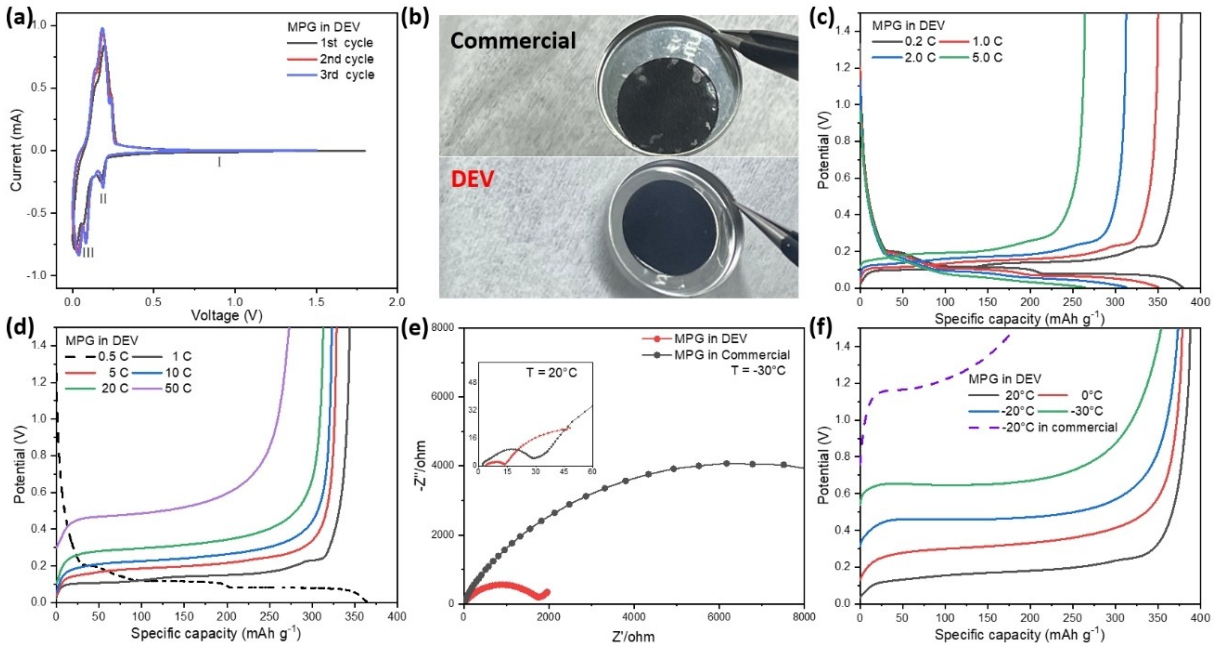

Figure 4. a) Initial 3 CV curves of the MPG measured at a scan rate of 0.05 mV s^{-1}, b) wettability of the electrodes in different electrolytes. c) GCD curves of MPG measured at different rates, d) Li-output curves of MPG measured at room temperature with different C rates after 0.5 C lithium insertion, e) EIS tests for MPG measured at 20 °C (the inset) and −30 °C in DEV and the commercial electrolytes, f) Li-output curves of MPG measured at different temperatures at 2 C after 0.2 C lithium insertion at room-temperature.

Research Article
doi.org/10.1002/batt.202200499
Chemistry Europe
European Chemical Societies Publishing

contact angle exhibited for DEV on the surface of MPG electrode than the commercial electrolyte (Figure S9). Whereas for the commercial electrolyte, the electrode is obviously not well-wetted, which would greatly affect the formation of SEI layer in the first cycle and consequently affect the following cycle life. Moreover, poor wettability of MPG in the commercial electrolyte also leads to lower first-cycle capacity, as indicated in Figure 3(a).

In galvanostatic charge/discharge test of the initial three cycles (Figure S10), MPG in DEV electrolyte exhibits extremely stable charge/discharge capacity after the first lithiation process, and ~85% ICE[32] is obtained, only ~4% less than the pristine graphite measured in the commercial electrolyte. It can be deduced that the electrochemical active surface area of MPG may be similar to the pristine graphite, although the BET surface area is higher in MPG. This might be attributed to the good extensibility of graphite where the pores are closed after the electrode is highly pressed. The GCD tests of MPG that measured in DEV electrolyte at different C-rates are displayed in Figure 4(c). Compared with the data measured in the commercial electrolyte (248 mAh g^{-1}@2 C), an appreciable improvement of rate performance is detected and a high capacity of 263 mAh g^{-1} can be delivered at 5 C. This indicates that the alleviation of Li^+ intercalation resistance at electrode-electrolyte interface could effectively enhance the rate performance of graphite anode. Li-output performance of MPG electrode in DEV is shown in Figure 4(d). Although the MPG delivers almost the same capacity (~280 mAh g^{-1}) at 50 C and at extremely-high cut-off voltage (1.5 V) in the DEV and commercial electrolytes, it delivers much higher capacity at low cut-off voltage in the DEV electrolyte (200 mAh g^{-1}@0.6 V, at 50 C) than that in the commercial electrolyte (12 mAh g^{-1}@0.6 V, at 50 C). Furthermore, the broader plateau and lower initial voltage (0.30 V) suggest that the charge-transfer resistance is sharply reduced using DEV electrolyte, which is further confirmed by the EIS results shown in the inset of Figure 4(e), where the R_{ct} of MPG in DEV electrolyte (13.66 Ω) is less than that measured in the commercial one (28.49 Ω). This low charge-transfer resistance of MPG in the DEV electrolyte ensures fast charging/discharging performance of practical full cells.

The performance of LIBs at low temperature is another important parameter. As shown in Figure S11, for the commercial electrolyte, Li output capacity of PG electrode sharply drops to 169 mAh g^{-1} at −20 °C and nearly no capacity can be delivered at −30 °C. With temperature decreasing, the migration rate of ions decreases in all steps evidenced by EIS result.[10] Figure 4(e) shows the Nyquist plots of MPG electrodes measured in the commercial and DEV electrolytes. The R_{ct} measured at −30 °C in DEV is substantially lower than that in the commercial electrolyte (Figure S11), showing a superior lithiation/de-lithiation performance at the interface. This is further confirmed by a slight increase of de-lithiation platform (0.5 V) from 20 °C to −30 °C at 2 C-rate (Figure 4f). In addition, the high capacity of 352.9 mAh g^{-1} at −30 °C and 2 C indicates that lithium diffusion in MPG particles at low temperature is fast enough, which could prevent the accumulation of lithium on its surface and consequently avoid the growth of lithium dendrite. Benefited from the smooth migration of ions at the interface and the short diffusion path in the particle, MPG can be charged safely at low temperature. As shown in Figure 5(a), only a weak voltage drop can be detected even when the temperature decreases to −30 °C, this further indicates that solvents could be easily removed from the solvated ions and then enter the electrode. In addition, due to weak solvation energy between Li^+ and DOL solvent, the phenomenon that the solvated ions attack the electrode would be relieved greatly, which hinders SEI growth and prolongs the cycling life of the electrode. As shown in Figure 5(b), after initial charge-discharge cycles, MPG becomes stable and exhibits an excellent cyclic stability in DEV electrolyte. Even after 500 cycles, the MPG electrode still remains a high reversible capacity of 311 mAh g^{-1} at 2 C-rate. Whereas for the commercial electrolyte, the half-cell fails to work after 200 cycles even at low C-rate (0.5 C). This long cycle life and fast lithiation/de-lithiation ability are attributed to the collaboration of highly stable crystal structure, good wettability and weak solvation energy in the MPG-DEV system.

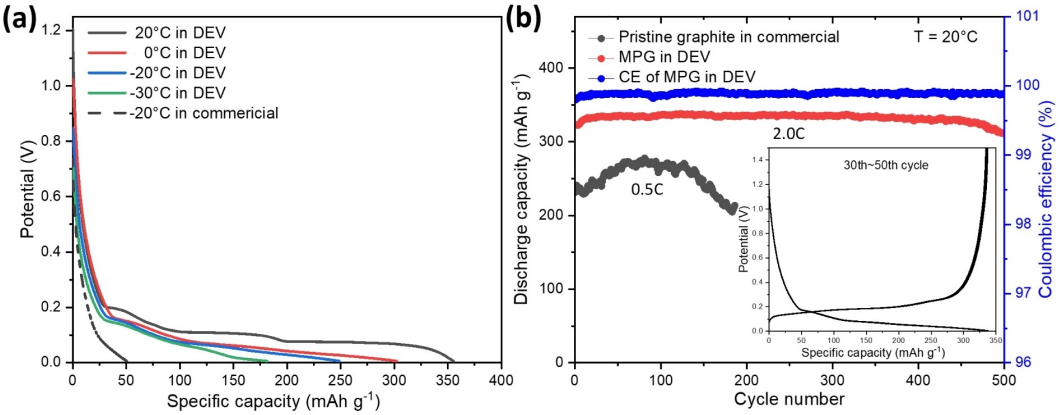

Figure 5. a) Lithium insertion curves of MPG measured at 0.2 C rate at different temperatures in DEV. b) Cycling stability of MPG measured at 2 C rate in DEV and 0.5 C rate in the commercial electrolyte. The inset in (b) exhibits the GCD curves of 30th to 50th cycles of MPG in DEV.

Conclusion

To alleviate poor rate performance caused by long diffusion path of ions in graphite anode, graphite containing numerous penetrated macropores with size of about 100 nm (MPG) is synthesized through oriented-etching with steam using NiO_x as catalyst. After activating, the lattice structure of graphite is maintained well in MPG and consequently a typical CV curve of graphite and a high ICE (85%) are displayed. Furthermore, benefiting from its porous structure, the Li-output capacity of MPG in half cell could reach 280 mAh g^{-1} at 50 C. Combined with DEV electrolyte with low solvation energy, MPG exhibits excellent rate and low-temperature tolerant performance due to smooth migration of ions at the interface and quick diffusion in the electrode, ~352.9 mAh g^{-1} capacity can be delivered at 2 C-rate and −30 °C. In addition, due to its good wettability in DEV, MPG exhibits an excellent cycling life (~94.2% capacity retention after 500 cycles at 2 C). We demonstrated that the product MPG has high potential to realize fast charging of the Li-ion batteries, especially at cool and cold environments.

Acknowledgements

This work was financially supported by the National Natural Science Foundation of China (22005124) and the Research Project Fund for Industrialization from Taizhou Institute for New Energy Research of Jiangsu University (201801), and Special Fund for Science and Technology Innovation of Jiangsu Province (BE2022610).

Conflict of Interest

The authors declare no conflict of interest.

Data Availability Statement

The data that support the findings of this study are available in the supplementary material of this article.

Keywords: charge transfer · lithiation · low-temperature tolerance · oriented-etch · porous graphite

[1] M. Armand, J. M. Tarascon, *Nature* **2008**, *451*, 652–657.
[2] V. Etacheri, R. Marom, R. Elazari, G. Salitra, D. Aurbach, *Energy Environ. Sci.* **2011**, *4*, 3243–3240.
[3] W. Cai, Y.-X. Yao, G.-L. Zhu, C. Yan, L.-L. Jiang, C. He, J.-Q. Huang, Q. Zhang, *Chem. Soc. Rev.* **2020**, *49*, 3806–3833.
[4] N. Yabuuchi, K. Kubota, M. Dahbi, S. Komaba, *Chem. Rev.* **2014**, *114*, 11636–11682.
[5] J. B. Goodenough, K.-S. Park, *J. Am. Chem. Soc.* **2013**, *135*, 1167–1176.
[6] H. Zhang, Y. Yang, D. Ren, L. Wang, X. He, *Energy Storage Mater.* **2021**, *36*, 147–170.
[7] K. Persson, V. A. Sethuraman, L. J. Hardwick, Y. Hinuma, Y. S. Meng, A. Van Der Ven, V. Srinivasan, R. Kostecki, G. Ceder, *J. Phys. Chem. Lett.* **2010**, *1*, 1176–1180.
[8] S. Z. Sheng, *J. Power Sources* **2006**, *161*, 1385–1391.
[9] G. A. Collins, H. Geaney, K. M. Ryan, *J. Mater. Chem. A* **2021**, *9*, 14172–14213.
[10] J. Xu, X. Wang, N. Yuan, J. Ding, S. Qin, J. M. Razal, X. Wang, S. Ge, Y. Gogotsi, *Energy Storage Mater.* **2019**, *23*, 383–389.
[11] Q. Cheng, R. Yuge, K. Nakahara, N. Tamura, S. Miyamoto, *J. Power Sources* **2015**, *284*, 258–263.
[12] J. Xu, X. Wang, N. Yuan, B. Hu, J. Ding, S. Ge, *J. Power Sources* **2019**, *430*, 74–79.
[13] N. Kim, S. Chae, J. Ma, M. Ko, J. Cho, *Nat. Commun.* **2017**, *8*, 1–10.
[14] P. Zhu, X. Yang, X. Li, N. Sheng, H. Zhang, G. Zhang, J. Sha, *Dalton Trans.* **2020**, *49*, 79–88.
[15] M.-H. Sun, S.-Z. Huang, L.-H. Chen, Y. Li, X.-Y. Yang, Z.-Y. Yuan, B.-L. Su, *Chem. Soc. Rev.* **2016**, *45*, 3479–3563.
[16] X. Feng, M. Ouyang, X. Liu, L. Lu, Y. Xia, X. He, *Energy Storage Mater.* **2018**, *10*, 246–267.
[17] J. Geder, H. E. Hoster, A. Jossen, J. Garche, Y. Denis, *J. Power Sources* **2014**, *257*, 286–292.
[18] Z. An, K. Shah, L. Jia, Y. Ma, *Appl. Thermal Engineering* **2019**, *160*, 113960.
[19] C. E. L. Foss, A. M. Svensson, S. Sunde, F. Vullum-Bruer, *J. Power Sources* **2016**, *317*, 177–183.
[20] B. Hu, X. Zhou, J. Xu, X. Wang, N. Yuan, S. Ge, J. Ding, *ChemElectroChem* **2020**, *7*, 716–722.
[21] S. S. Zhang, K. Xu, T. R. Jow, *Electrochim. Acta* **2003**, *48*, 241–246.
[22] X. Fan, X. Ji, L. Chen, J. Chen, T. Deng, F. Han, J. Yue, N. Piao, R. Wang, X. Zhou, *Nat. Energy* **2019**, *4*, 882–890.
[23] T. Deng, X. Zhou, *J. Solid State Electrochem.* **2016**, *20*, 2613–2618.
[24] R. Krishna, J. Wade, A. N. Jones, M. Lasithiotakis, P. M. Mummery, B. J. Marsden, *Carbon* **2017**, *124*, 314–333.
[25] X. Luo, H. Zheng, W. Lai, P. Yuan, S. Li, D. Li, Y. Chen, *Energy Environ. Mater.* **2022**, https://doi.org/10.1002/eem2.12402..
[26] J. Xu, R. Zhang, J. Wang, S. Ge, H. Zhou, Y. Liu, P. Chen, *Carbon* **2013**, *52*, 499–508.
[27] T. Deng, X. Zhou, *Mater. Lett.* **2016**, *176*, 151–154.
[28] S. Uchida, M. Ishikawa, *J. Power Sources* **2017**, *359*, 480–486.
[29] J. Xu, J. Ding, W. Zhu, X. Zhou, S. Ge, N. Yuan, *Sci. China Mater.* **2018**, *61*, 371–381.
[30] T. Rauhala, J. Leis, T. Kallio, K. Vuorilehto, *J. Power Sources* **2016**, *331*, 156–166.
[31] G. Yang, X. Li, Z. Guan, Y. Tong, B. Xu, X. Wang, Z. Wang, L. Chen, *Nano Lett.* **2020**, *20*, 3836–3843.
[32] J. Holoubek, H. Liu, Z. Wu, Y. Yin, X. Xing, G. Cai, S. Yu, H. Zhou, T. A. Pascal, Z. Chen, *Nat. Energy* **2021**, *6*, 303–313.
[33] Z. Li, Z. Jian, X. Wang, I. A. Rodríguez-Pérez, C. Bommier, X. Ji, *Chem. Commun.* **2017**, *53*, 2610–2613.
[34] Y. Zheng, T. Qian, H. Ji, X. Xia, J. Liu, Y. Zhu, C. Yan, *Adv. Mater.* **2021**, *33*, 2102634.
[35] S. Grugeon, P. Jankowski, D. Cailleu, C. Forestier, L. Sannier, M. Armand, P. Johansson, S. Laruelle, *J. Power Sources* **2019**, *427*, 77–84.

Manuscript received: November 16, 2022
Revised manuscript received: January 21, 2023
Accepted manuscript online: January 23, 2023
Version of record online: February 7, 2023